

# DS1 Ion Propulsion Emissions Characterization

Michael D. Henry (Michael.D.Henry@jpl.nasa.gov)  
David E. Brinza (David.E.Brinza@jpl.nasa.gov)  
Jet Propulsion Laboratory  
California Institute of Technology  
4800 Oak Grove Drive  
Pasadena, CA 91109-8099

*Abstract*—The Deep Space One mission is demonstrating the long-duration use of an Ion Propulsion Subsystem (IPS). The NASA Solar Electric Propulsion Technology Applications Readiness Project developed the NSTAR Diagnostics Package (NDP) to monitor the effects of the IPS on the spacecraft environment. The NDP measures contamination, plasma characteristics, electric fields, and magnetic fields.

This paper describes the different electro static and electro magnetic emissions of the Ion engine for each of the thrust levels the engine has operated in space and in the test chamber. It shows the E and B fields data from the spectrometer and the associated time domain samples. It identifies the unexpected differences between the engine emissions for different thrust levels. It shows the peculiarities of the transitions from one thrust level to another. And it shows the differences in the space and ground test emissions. Examples of other spacecraft emissions will be shown for comparisons to the Ion engine emissions.

## TABLE OF CONTENTS

1. INTRODUCTION
2. NDP CHARACTERIZATION DESCRIPTION
3. ELECTRO STATIC/MAGNETIC
4. AC MAGNETIC
5. TIME DOMAIN E & B
6. CONCLUSIONS

## 1. INTRODUCTION

NASA's New Millennium Deep Space One (DS1) mission is the first spacecraft to rely on solar electric propulsion (SEP) as the primary propulsion system. DS1 was launched on October 24, 1998. It successfully flew by asteroid 9969 Braille on July 28, 1999. It is currently on its way to the comet Borrelly for a 2001 fly-by, as part of an extended mission.

The NASA Solar Electric Propulsion Technology Applications Readiness Project developed the NSTAR Diagnostics Package (NDP) to monitor the effects of the IPS on the spacecraft environment. The NDP measures

contamination, plasma characteristics, electric fields, and magnetic fields.

## 2. NDP CHARACTERIZATION DESCRIPTION

The NSTAR diagnostics effort includes ground test, modeling, and flight measurements to assess the environmental impact of ion-thruster operations on spacecraft payloads (instruments) and sub-systems. The EMI/EMC ground test and flight measurement approaches are described below.

### 2.1 Ground Test Diagnostics

The NSTAR thruster element included development and test of engineering model thruster (EMT) and flight thruster systems. The NSTAR contractor, Hughes Electron Dynamics Division, delivered flight thrusters with significant design heritage to the 30-cm xenon ion thrusters developed by the NASA Glenn Research Center[1]. Various ground tests were conducted throughout the NSTAR project, culminating with flight thruster compatibility tests with the DS1 spacecraft prior to launch. The following sections describe these NSTAR tests in the context of diagnostic measurements.

*2.1.1 Early EMT Testing*—The early EMT tests were moderate in duration (hundreds of hours up to 2000 hr) to characterize erosion characteristics, thruster performance, etc. During this phase, design details and operating points of the NSTAR thruster were adjusted to enhance thruster reliability and performance for long duration operation. Since minor changes to thruster design may substantially alter the contamination, EMI, or plasma conditions associated with the thruster, very few quantitative diagnostic tests were planned. A few witness materials were examined and qualitative measurements of EMI were performed; however, these tests remain geared to thruster evaluation.

*2.1.2 Life Demonstration Test*—The NSTAR program performed a life demonstration test (LDT) of an ion engine that successfully demonstrated the ability of the NSTAR EMT to operate at full power for more than 8000 hours[2]. The LDT afforded an excellent opportunity to collect contamination data and to establish flight plasma sensor

design and performance requirements. Ground tests produced “chamber effects” that can interfere with the measurement of the relevant environments. interaction measurements; however, there were mitigation approaches that provided useful data. Much of the data gathered from the LDT was of comparative nature: before and after grid mass, thrust vector stability, engine efficiency, etc. The NSTAR diagnostics element characterized the magnitude and stability of the DC magnetic field produced by the EMT before and after the LDT.

**2.1.3 EMI/EMC**—As part of the acceptance process, the flight units underwent characterization of DC magnetic fields, measurement of DC and AC magnetic fields during operation, measurement of AC electric fields during operation, and assessment of plume effect on RF communications. These tests were performed at JPL and at the NASA Glenn Research Center. Included in this test was a spacecraft-level test in which the NSTAR PPU was operated into a resistive load.

**DS1 IPS Compatibility Test**—The full flight system functional test of the IPS on DS1 was conducted in vacuum following spacecraft thermal vacuum testing. This test also provided an opportunity to characterize plasma and electric/magnetic fields associated with operation of the ion thruster in flight configuration. IDS hardware was integrated and fully operational for the IPS compatibility test. Although the IPS operating time was limited, IDS successfully captured plasma and fields data in this test. Correlation with flight data provides insight into chamber effects on potential and EMI measurements.

## 2.2 IPS Diagnostics Subsystem on DS1

A suite of 12 diagnostic sensors was integrated into the IDS shown in Figure 1. IDS was located adjacent to the NSTAR ion engine on the DS1 spacecraft.

**2.2.1 IDS Architecture**—IDS consists of two interconnected hardware units: the Diagnostics Sensors Electronics Unit (DSEU) and the Remote Sensors Unit (RSU). The DSEU component of the IDS has considerable heritage to SAMMES, a modular instrument architecture developed by BMDO[3,4]. A block diagram for the IDS is shown in Figure 2. The IDS is a highly integrated instrument package with a single +28 VDC power and dual MIL-STD-1553 serial communications interface to the DS1 spacecraft. The compact IDS instrumentation package weighed just 8 kg and required 21 W for full operation.

The IDS contains two separate processor elements: the DSEU microprocessor and the fields measurement processor (FMP)[5]. The DSEU microprocessor supports the communications interface with DS1, controls serial communications with the FMP, and digitizes and controls

the sensors within the RSU. The IDS operates as a remote terminal on the DS1 MIL-STD-1553 serial bus. Telemetry from the RSU sensors is collected on 2-second intervals and placed in selected 1553 subaddresses for transmission to DS1. Configuration messages are transmitted to the DSEU to select active sensors within the RSU and FMP and to establish sweep ranges and gains for these sensors. Configuration messages to the FMP are passed through the DSEU to the FMP directly. The DSEU polls the FMP for data at half-second intervals. In the typical FMP “scan” mode operation, a block of sensor data is transmitted at 16-second intervals. Occasionally, the FMP will transmit 1-second waveforms sampled at 20 kHz from the plasma wave and search sensors and 20 Hz from the flux-gate magnetometers. These “burst” events can be commanded or initiated via internal triggering within the FMP.

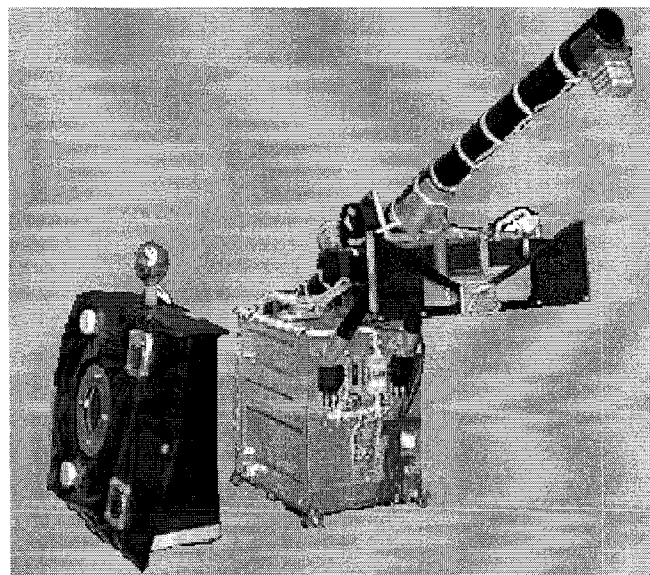


Figure 1. IPS Diagnostics Subsystem Hardware

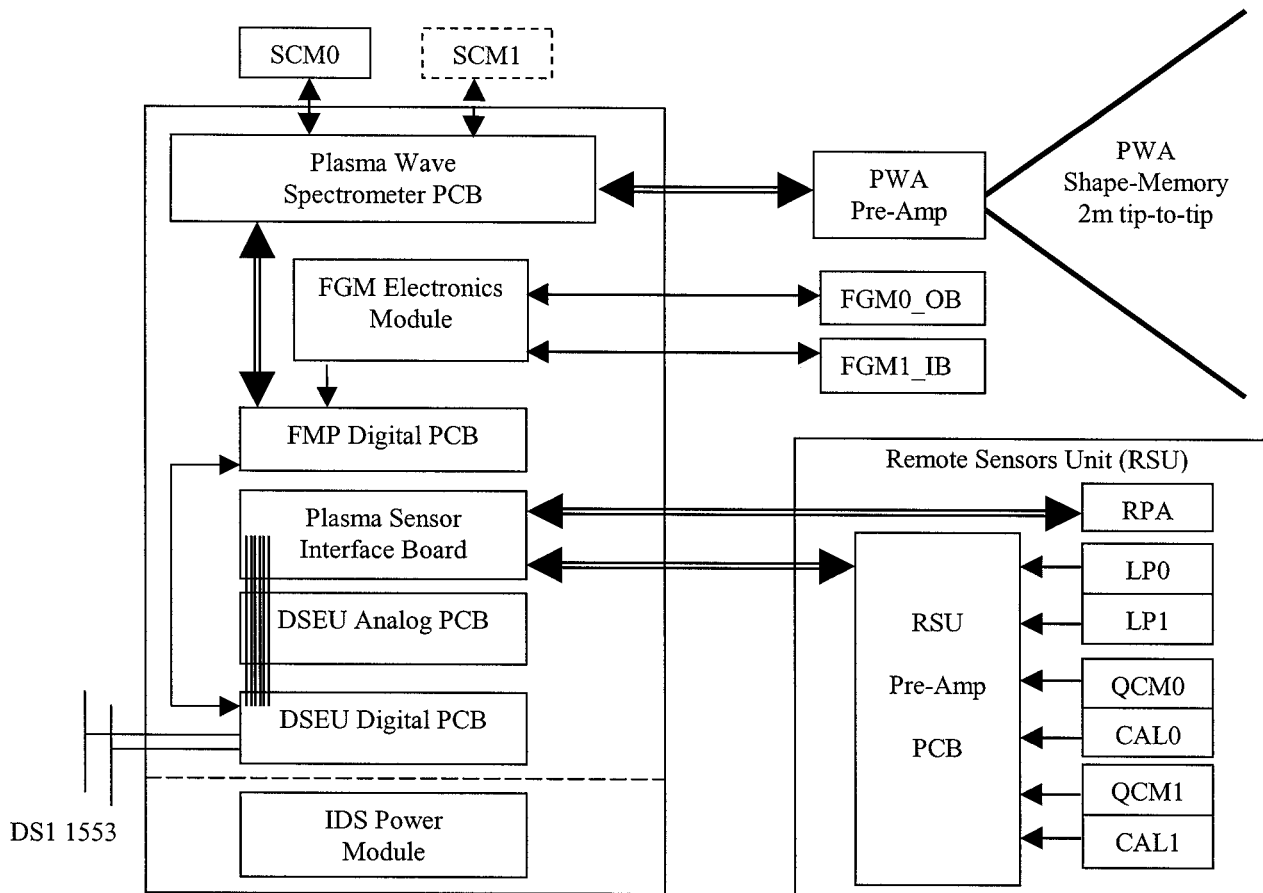


Figure 2. IPS Diagnostics Subsystem Block Diagram

### 3. ELECTRO STATIC/MAGNETIC

#### Ground Test-

An IPS Compatibility Test (ICT) with the DS1 spacecraft was performed in the JPL 25-foot space simulator facility in February 1998. During the ICT, the IPS was briefly operated at TH0 (ML6), TH7-8 (ML55-ML62) and TH14 (ML104) thrust levels. The IDS Engineering Model, which included the flight Plasma Wave Antenna (PWA) pre-amplifier and Plasma Wave Spectrometer (PWS) board from TRW, was used in the ICT. The IDS used rigid, non-flight 2-meter tip-to-tip wire antenna to monitor electric field signals. A flight-like search coil was used to collect AC magnetic field data.

At the time of the DS1 ICT, the IDS software manager was not on-board, so DS1/IDS command and data communications were invoked by primitive commands to the DS1 MIL-STD-1553B bus controller hardware. IDS could not transmit time-domain data in the "burst" mode, since no processing of the IDS bus traffic was performed by the DS1 flight computer at this time. Data from IDS were captured by an external MIL-STD-1553B bus monitor. Therefore, the DS1 test conductor only executed IDS

configuration or gain commands during periods of low spacecraft activity. No IDS commanding was performed during IPS thrust operations. The IDS team had prepared several PWS gain commands in preparation for the ICT. For the initial ML6 operations, the PWS gain was set at a relatively low level. Upon examination of the PWS data, the PWS gain was set to a high level for the remainder of the ICT.

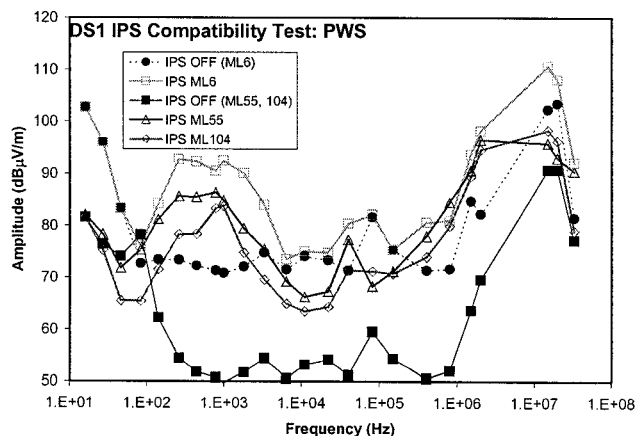


Figure 3.1 Plasma wave spectrum for ICT thrust levels

PWS electric-field data obtained during the DS1 ICT is shown in Figure 3.1. A few features are readily noted in the power spectra. A large peak appears in the 1 MHz to 15 MHz region, attributed to IPS electron plasma frequency noise. A lesser peak is seen in the 200 Hz to 4 kHz region, the source of this signal is not yet understood. The amplitude of the PWS signal is less than  $0.1 V_{p-p}/m$  except near 15 MHz, where the signal approaches  $0.3 V_{p-p}/m$ . Note that there is little signal observed in the 10 kHz to 300 kHz frequency region during the ICT.

*Flight Measurements-*

For purposes of comparison with ground measurements made during the DS1 ICT, data from a brief IPS activity on DS1 to assess power production from the SCARLET solar arrays is presented. This DS1 test, referred to as “S-Peak”, operated the IPS for a relatively brief interval (less than 40 minutes total). The IPS is always started with high cathode flow rates and the characteristic time to reach steady-state flow conditions is generally several hours. Therefore, this brief S-Peak test most closely resembles the IPS conditions during the ICT. Due to the spacecraft to Sun range, though, DS1 was not able to achieve the ML104 maximum level witnessed in the ICT.

PWS electric-field data obtained during the “S-Peak” test is shown in Figure 3.2 below. Since time-domain data collection was enabled to capture high-amplitude events during the S-Peak test, the PWS gain settings were lower than that for the DS1 ICT. The PWS noise “floor” for S-Peak is about  $0.01 V_{p-p}/m$ . The high-frequency feature between 1 MHz and 15 MHz is about 10dB higher in amplitude in the flight S-Peak than what was observed in the ground-based ICT. Unlike the ICT, essentially no signal amplitude is observed between 200 Hz to 4 kHz during S-Peak. A substantial signal is observed in the 10 kHz to 300 kHz frequency region in the S-Peak data, in contrast to the minimal signal observed in this frequency regime during ICT. Both the ICT and S-Peak data sets appear to show an amplitude “dip” between 300 kHz and 2 MHz.

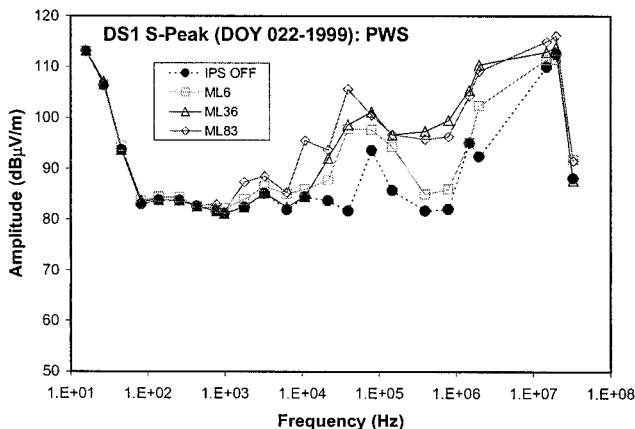


Figure 3.2 Plasma wave spectrum for S-Peak thrust levels

Characteristic plasma wave signal measurements under IPS steady-state thrust conditions were obtained during IPS Acceptance Tests IAT1 and IAT2. The results for IAT1 are shown in Figure 3.3. The plot symbol size approximates the amplitude error bars at high signal levels. The PWS signal might be expected to correlate with the thrust level for the IPS. The data in Figure 3.3 clearly shows no straight-forward correlation between plasma noise amplitude and IPS thrust level. Note that the highest thrust level (TH12, ML90) has a plasma wave spectrum almost the same as that for TH3 (ML27). The highest plasma noise in IAT1 is observed for TH11 (ML83). Maximum signal levels, at 40 kHz are about  $0.2 V_{p-p}/m$  and from 2 MHz to 15 MHz are approximately  $0.5 V_{p-p}/m$ , similar to amplitudes observed in the S-Peak data. The behavior in the low frequency region (below 10 kHz) with thrust level is not well understood, but could be due to inter-modulation between switching power supply modules within the IPS power-processing unit.

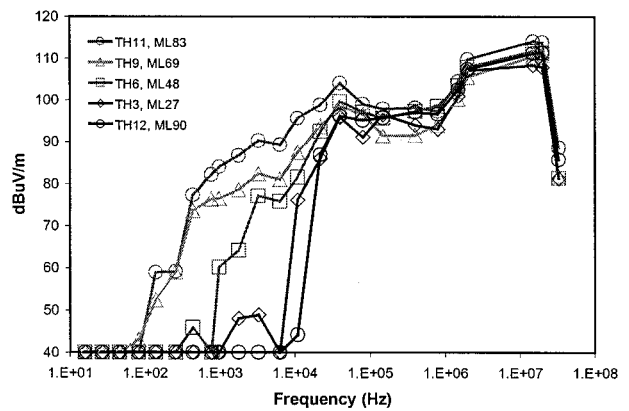


Figure 3.3 Plasma wave spectra for IAT1 mission levels

Plasma wave noise measurements obtained during the lower thrust level IAT2 are shown in Figure 3.4. Note that the lowest thrust level (TH0, ML6) has a noise spectrum almost as high as that for TH4 (ML34). The spacecraft noise level just prior to initiation of IAT2 is plotted as a solid black line in the Figure. The spacecraft noise includes a signal from an unknown source in the 2 kHz to 7 kHz region. This signal appears to be attenuated by thruster operations at ML 13 through ML 26. Maximum signal levels, at 40 kHz and 2 MHz to 15 MHz approach  $1V/m$ . Again a characteristic “dip” in the spectrum is observed in the 300 kHz to 1 MHz frequency region.

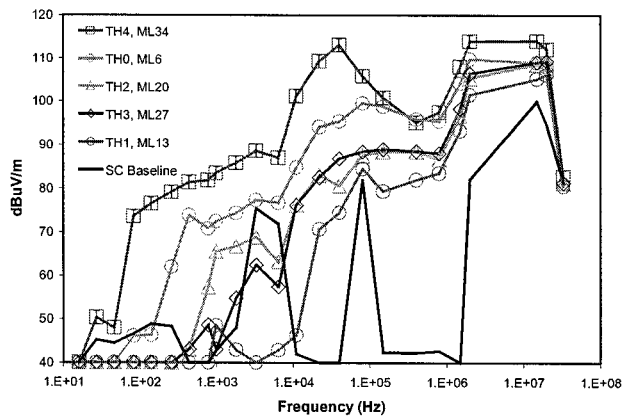


Figure 3.4 Plasma wave spectrum for IAT2 mission levels

The plasma noise from the IPS occasionally changes rather dramatically during thrust level transitions. Upon transition to a higher thrust level, the IPS is designed to first increase the xenon flow, then increase the ion beam current and other IPS electrical parameters. Increased xenon flow, at a fixed beam current, will increase the production of charge-exchange xenon. This charge-exchange xenon plasma behaves as an electrically conducting medium for the plasma noise. An dramatic example of this behavior is illustrated in Figure 3.5 below. The amplitude of the plasma noise in the 22 kHz band increases by a 1000-fold during the 2-minute transition from ML20 to ML27. Note that the steady-state plasma wave signatures for these two thrust levels are within a factor of two of each other.

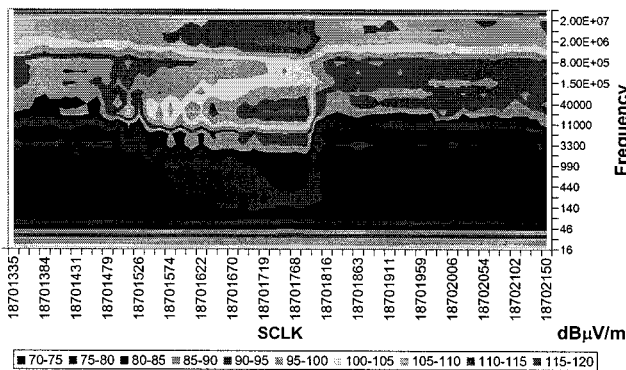


Figure 3.5 Plasma wave spectrogram for IPS transition from ML20 to ML27.

The transition between IPS ML83 to ML90 is shown in Figure 3.6 below. In this case, the plasma noise decreases dramatically in the lower frequency region (<10 kHz). This phenomenon has been repeated in ground test by reducing neutralizer flow or discharge current. In the ground test, it is possible for a secondary plasma sheath associated with the chamber walls to envelope a portion of the antenna. In flight, the higher noise level at ML83 might be due to the amount of residual xenon available for producing a noisy plasma discharge within the neutralizer. Further experimentation in flight will not occur until after

completion of the extended science mission, since reduced xenon flow represents an erosion risk to the cathodes. (A common plenum tank controls both the NSTAR IPS neutralizer and discharge cathodes, so the erosion risk exists for both devices.)

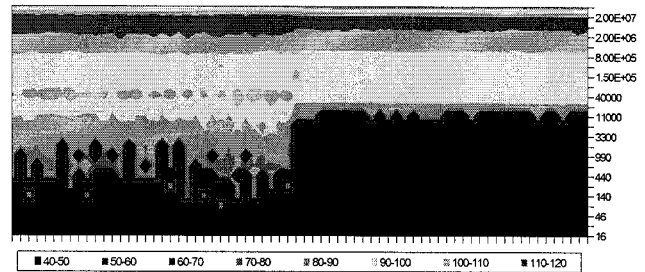


Figure 3.6 Plasma wave spectrogram for IPS transition from ML83 to ML90.

needed.

#### 4. AC MAGNETIC

##### Ground Test-

In addition to the electric field measurements, the IDS made simultaneous measurements of AC magnetic fields during the DS1 IPS Compatibility Test (ICT). In spite of setting the gain to the maximum level after the TH0 (ML6) initial firing of the IPS, no signals above the noise floor were recorded during the test. Prior to and subsequent to IDS delivery to the ICT, the IDS engineering model search coil easily detected AC magnetic field stimuli applied with a small excitation coil. The absence of AC magnetic signature in the ICT ground test is very surprising, given the amplitudes observed in flight.

Measurements were made with engineering model search coil in NSTAR characterization tests CT31 and CT36 capturing signals with a fast digital oscilloscope. As seen in Figure 4.1 below, the search coil shows a weak response to transient events, such as the IPS engine start, but does not show much electromagnetic interference (EMI) noise with steady-state engine operations. Whether the lack of strong AC magnetic signals is due to chamber effects or EMI-shielding or grounding considerations is under debate.

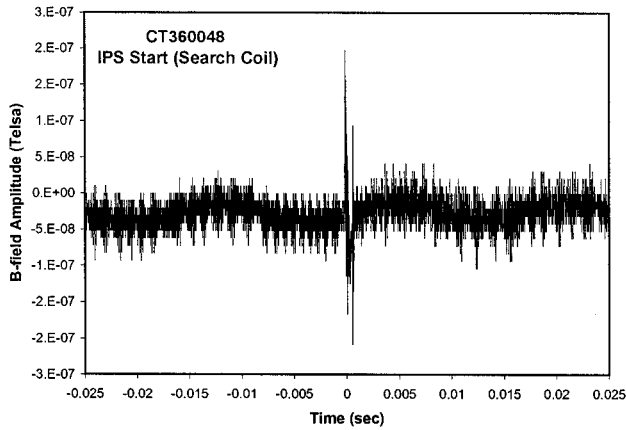


Figure 4.1. Response of the search coil magnetometer to IPS start during ground testing.

*Flight Measurements-*

AC magnetic field data recorded by the IDS engineering search coil (SC0) during IAT1 is shown in Figure 4.2. Some of the characteristic trends observed in the electric field data (Figure 3.3) are also seen for the magnetic (B-fields). The highest amplitude B-fields are found at ML83 in the 1 kHz to 5 kHz region. The peak amplitude for ML90 is 10 dB below that of ML83, as found in the E-field spectra. The lowest B-fields in IAT1 are found at ML27 and ML48, which differs from the E-field measurements where ML90 was the least noisy operating point. The lower-frequency signals (50 Hz to 200 Hz) appear to have less variation with operating level and are not consistent with the order witnessed in the 1 kHz to 5 kHz region. Until the IAT2 test was performed, the nature of the low-frequency magnetic field signals were not understood.

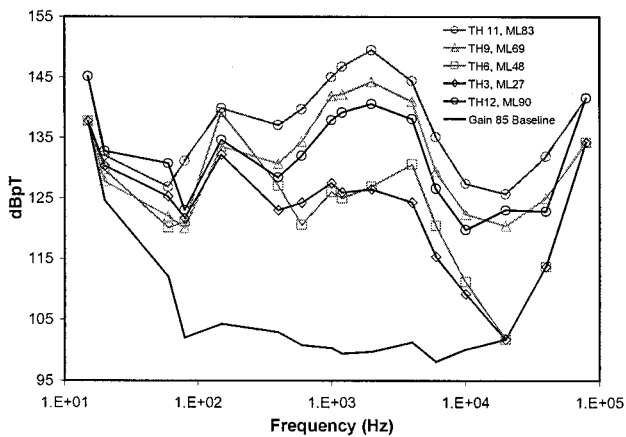


Figure 4.2 AC magnetic spectra for IAT1 mission levels

Data obtained during the DS1 IAT2 activity is shown in Figure 4.3. The figure shows the relative contribution to a known non-IPS source of EMI on the DS1 spacecraft, the engine gimbal assembly (EGA) stepper-motors for performing thrust vector control of the IPS engine. IAT2 included special EGA motion patterns for magnetic field and

charge-exchange plume mapping experiments (data still under analyses). The attitude control system software maintained DS1 pointing using only the reaction control subsystem (RCS) hydrazine thrusters during this period of IAT2. As a result, the DS1 search coils could distinguish between EMI produced by the EGAs and the IPS during ion engine operations. Note that the EGA noise amplitudes are comparable to IPS noise, though at much lower frequency (<400 Hz). The IPS

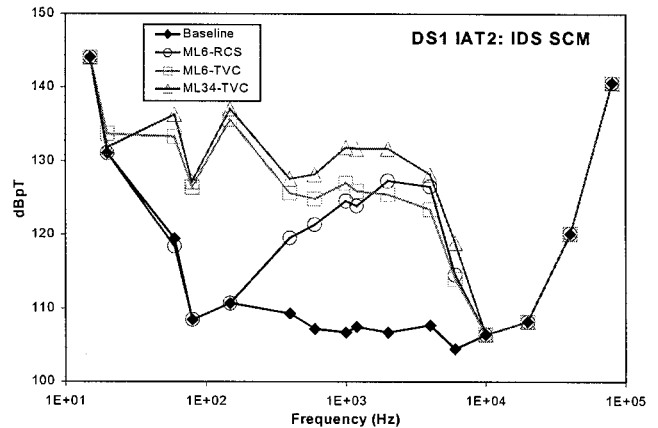


Figure 4.3 AC magnetic field spectra for IAT2 mission levels

5. TIME DOMAIN E & B FIELDS

*Ground Test-*

As indicated in section 3.1, the DS1 flight software to control the IDS was not available during the ICT. Time-domain data from the plasma wave antenna and search coil sensors could not be captured during this integrated ground test of DS1 and IPS. Time-domain waveform data from plasma wave antennas were recorded during NSTAR developmental and characterization tests using flight-like sensors and laboratory digital oscilloscopes.

Examples of a typical high-amplitude IPS generated event are shown in Figure 5.1 and Figure 5.2. This event occurs during discharge ignition during IPS start-up. An actively amplified monopole antenna detected the data in Figure 5.1. The amplitude of this event is 8  $V_{p-p}/m$ . Data shown in Figure 5.2 was simultaneously recorded with a 2-m tip-to-tip dipole antenna with an engineering model IDS PWA pre-amplifier. Notice that amplitude recorded by the dipole antenna is only about 2  $V_{p-p}/m$ , about a factor of 4 less than the monopole signal.

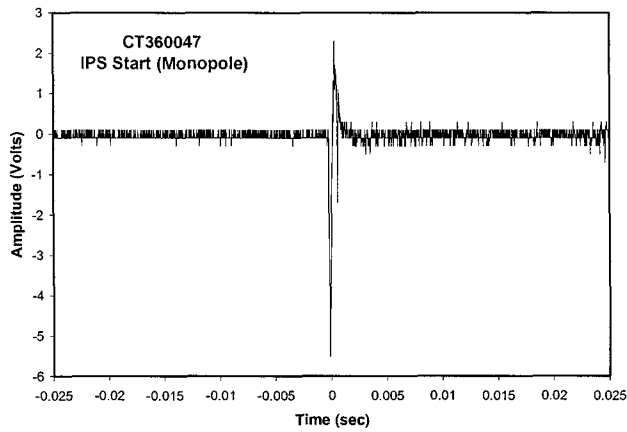


Figure 5.1 IPS ignition in CT36 ground test (monopole)

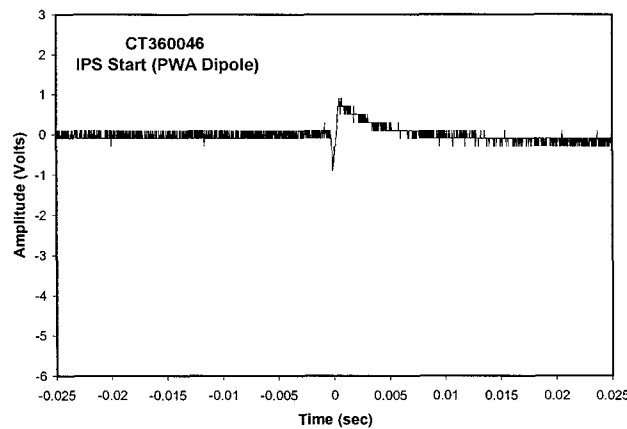


Figure 5.2 IPS ignition in CT36 ground test (PWA dipole)

The IDS recorded several IPS ignition events in flight. Data for a typical IPS ignition is shown in Figure 5.3 below. The peak signal at  $t=0$  seconds is approximately 1 V/m, consistent with the level observed in PWA dipole measurement from the CT36 ground test. After the ignition event, the noise from the IPS plasma is clearly visible in the IDS PWA data. Simultaneous magnetic field data for IPS ignition from the IDS search coil magnetometer is displayed in Figure 5.4. Peak field strengths of about 50,000 nT are observed for IPS discharge ignition.

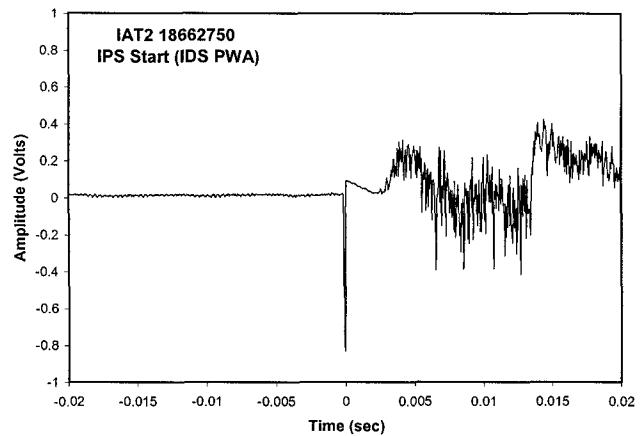


Figure 5.3 E-field transient signal for flight IPS ignition

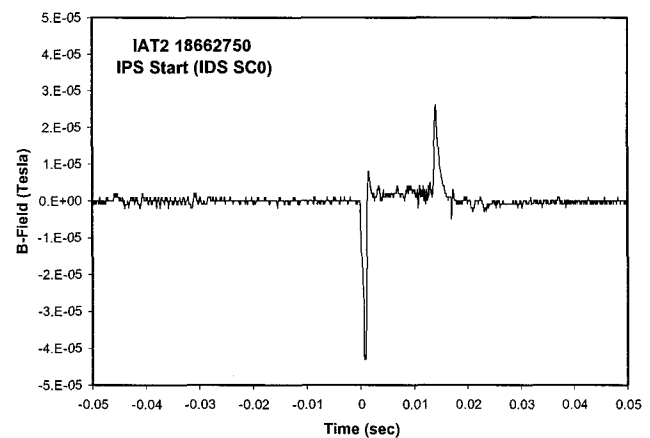


Figure 5.4 B-field transient signal for flight IPS ignition

The IPS can also produce high-amplitude transient field events when a momentary ionization arc between the grids induces a “recycle” event. The NSTAR power processor unit will disable the ion beam power supplies within a few microseconds of a fault condition in the output. Within a second of disabling the beam supplies, the power processor gradually restores the beam supplies to the thrust level. Examples of the E- and B-field transients for a recycle event are shown in Figures 5.5 and 5.6 respectively.

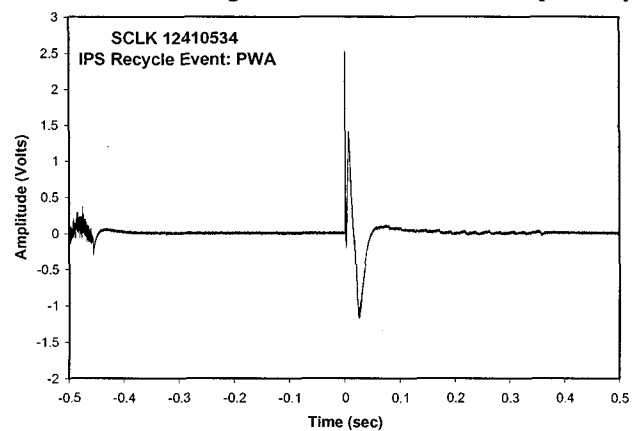


Figure 5.5 E-field signature for IPS recycle at  $t=-0.45$ . The

large signal near  $t=0$  is due to hydrazine thrusters firing.

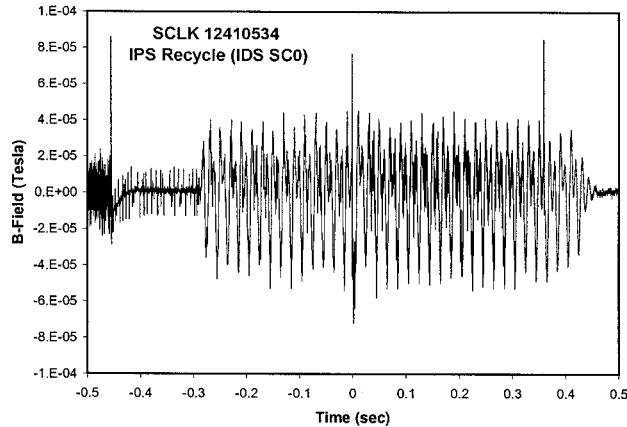


Figure 5.6 B-field signature for IPS recycle at  $t=-0.45$ . The large signals from  $t=-0.3$  to  $0.45$  are from gimbal actuators. The transient spike at  $t=0$  is from the RCS thruster valve.

[The IPS stops at  $t=-0.45$  sec, an RCS thruster firing occurs at  $t=0$ , the low frequency magnetic oscillations between  $t=-0.3$  and  $t=0.45$  are due to the engine gimbal assembly motors.]

The DS1 reaction control system (RCS) thrusters are responsible for some of the largest amplitude transient signals observed by the IDS. As shown in Figures 5.7 and 5.8, the RCS-produced signals are substantial. Electric-field amplitudes in excess of  $2 \text{ V}_{p-p}/\text{m}$  are typically observed for the RCS thruster firings. The origin of this high-amplitude signal is not fully understood, but a strong candidate is the ability of low-density gas flows to discharge electrically charged surfaces. The plasma wave antenna will become moderately charged due to the photoelectric effect. Some variation of the e-field amplitude has been observed with changes in sun angle on DS1, supporting the possibility that charge dissipation is responsible for the signals. The magnetic field signals in Figure 5.8 are attributed to the solenoid valve drive pulses. The various thruster firing combinations on DS1 yield unique, but reproducible, magnetic field signatures.

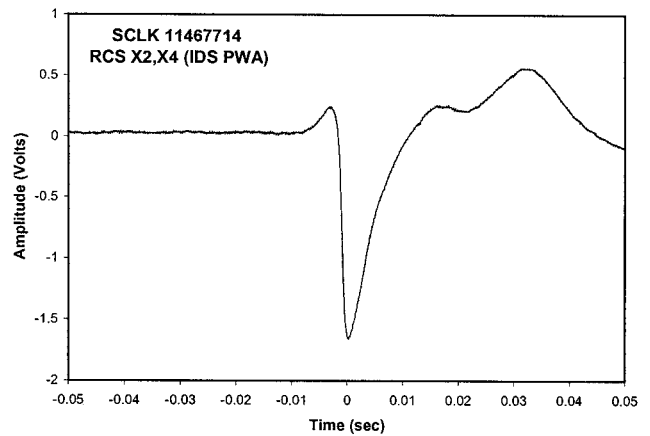


Figure 5.7 E-field signature for RCS thrusters firing at  $t=0$ .

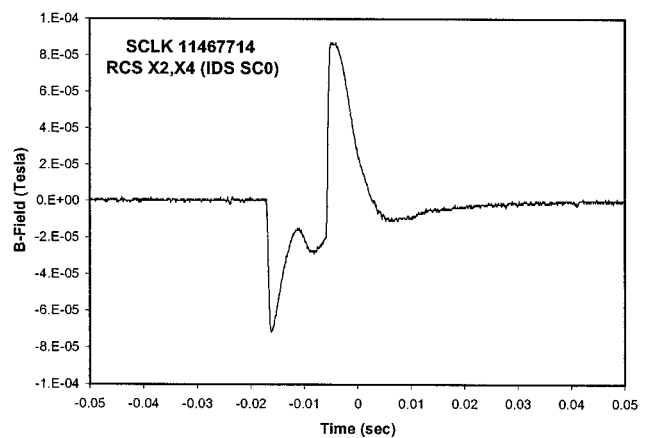


Figure 5.8 B-field signature for RCS thrusters firing at  $t=0$ .

On several occasions, strong E-field transient events have been recorded by the IDS without RCS or IPS operations. These E-field signals do not have a simultaneous magnetic signature, suggesting a momentary plasma discharge. Such events have been attributed to hypervelocity impacts and have been observed in many space missions (Pioneer, Voyager, Galileo). Figures 5.9 and 5.10 provide an example of such an event on DS1.

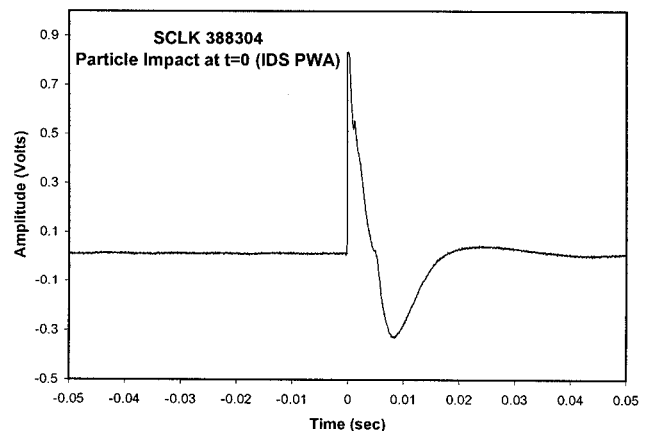


Figure 5.9 E-field signature for particle impact at  $t=0$ .

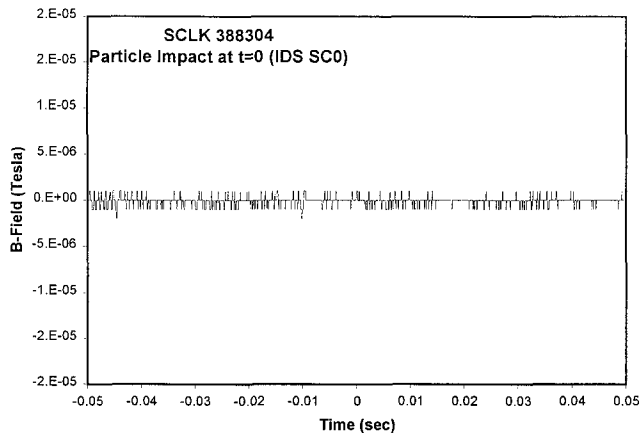


Figure 5.10 B-field recording for particle impact at  $t=0$ .

## 6. CONCLUSIONS

DS1 provided an excellent opportunity for in-depth investigation of interactions of an ion propulsion system with an interplanetary spacecraft in flight. The NSTAR project recognized the importance of characterizing the local environment due to IPS operations and chose to fly a diverse set of instrumentation. The sensors were selected to capture the range of expected signals from the IPS. Hence, the sensor sensitivity and response characteristics are generally less than what is found in space-science instrumentation. Notable exceptions to the above statement are the flux-gate magnetometers provided by the Technical University of Braunschweig. The FGMs have performed exceptionally well throughout the mission and may have detected a weak (2 nT) magnetic signature during the flyby of Asteroid Braille[23]. The IDS has succeeded in collecting the data required to characterize the local environment and effects induced by the IPS operating on DS1.

The IDS Plasma Wave Spectrometer characterized the electrostatic wave and electromagnetic noise environments produced by the IPS and other DS1 subsystems. A large volume of both spectral and time-domain data were obtained throughout the DS1 mission, especially during IPS operations. There is not a direct correlation of noise amplitude with IPS operating power. The IPS noise levels are bounded as follows:

- IPS E-field continuous noise:  $< 1$  V/m,  $< 15$  MHz.
- IPS E-field transient:  $< 2$  V/m for  $< 1$  ms.
- IPS B-field continuous noise:  $< 10$   $\mu$ T,  $< 10$  kHz.
- IPS B-field transient:  $< 200$   $\mu$ T for  $< 2$  ms.

Limits for the major DS1 subsystem noise sources, namely the hydrazine reaction control subsystem (RCS) thrusters and engine gimbal actuators (EGAs), are bounded by:

- RCS thruster E-field transient:  $< 5$  V/m for  $< 10$  ms.
- RCS thruster B-field transient:  $< 200$   $\mu$ T for  $< 40$  ms.

- EGA B-field continuous noise:  $< 10$   $\mu$ T, at 100 Hz.
- EGA B-field transient:  $< 100$   $\mu$ T for  $< 1$  s.

From a spacecraft systems-engineering perspective, the IPS does not produce *peak* electromagnetic or electrostatic noise beyond that of other spacecraft subsystems[5]. Note that, when operating, the IPS produces noise continuously; conversely, the other spacecraft sources are typically transient in nature. A major finding is the IPS does not introduce any interference in spacecraft communications or other subsystem operations.

The research described in this paper was carried out at Jet Propulsion Laboratory, California Institute of Technology, under a contract with the National Aeronautics and Space Administration

## REFERENCES

- [1] Christensen, J. A., Freick, K. J., Hamel, D. J., Hart, S. L., Norenberg, K. T., Haag, T. W., Patterson, M. J., Rawlin, V. K., Sovey, J. S. and Anderson, J. R., Design and fabrication of a flight model 2.3 kW ion thruster for the Deep Space 1 Mission, *AIAA Paper 98-3327*, 1998.
- [2] Polk, J. E., Anderson, J. R., Brophy, J. R., Rawlin, V. K., Patterson, M. J., Sovey, J., and Hamley, J., An overview of the results from an 8200 hour wear test of the NSTAR ion thruster, *AIAA Paper 99-2446*, 1999.
- [3] Arnold, G. S., Brinza, D. E., Joshi, P., Keener, D. N., Space active modular materials experiment, *SPIE Proc. Vol. 3427*, 225, 1998.
- [4] Joshi, P., Malonson, M., Green, B. D., McKay, J., Brinza, D. E. and Arnold, G. S., Space Environment and Effect Monitoring Instrumentation for Small Satellites, *J. Spacecraft and Rockets*, 35(6), 821, 1998.
- [5] Henry, M. D., Brinza, D. E., Mactutis, A. T., McCarty, K. P., Rademacher, J. D., vanZandt, T. R., Johnson, R., Musmann, G. and Kunke, F., NSTAR Diagnostics Package Architecture and Deep Space One Spacecraft Event Detection, *IEEE 2000 Aerospace Conference Paper 11.0502*, 2000.